Instabilities in charged tori

Author: Marc Herranz i Alié
Facultat de Física, Universitat de Barcelona, Diagonal 645, 08028 Barcelona, Spain.

Advisor: Alberto Fernández-Nieves

Abstract: This report aims to shed light on the different instability regimes of charged toroidal droplets. Firstly, we have studied the shrinkage and breakup of neutral tori through Rayleigh-Plateau instabilities. When charged, electrical stresses can overcome surface tension stresses leading to droplet expansion. At even higher voltage, tori can develop Saffman-Taylor instabilities, which result in viscous fingering. Remarkably, at high enough potential, these viscous fingering branch out, giving rise to a magnificent dendritic-growth behaviour.

I. INTRODUCTION

In nature, droplets can be seen when expelled by aquatic animals through their blow hole, near the coastline when waves collapse, or when falling from the sky in rainy days.
Nevertheless, despite being created via different mechanisms, all droplets ultimately tend to the same shape. This is due to surface tension, which favours minimizing the surface for a given volume.
However, in the presence of external forces, a droplet can adapt transient non-spherical shapes. But once they disappear, surface tension rounds all liquid drops up. Consequently, the generation of droplets with a non-minimal surface is challenging.

Given its symmetry, a donut-like shape can be fully described through two parameters; the distance from the rotation axis R_o, and the radius of the tube a_o (see Fig.1a). The slenderness of the torus solely depends on the ratio of these quantities, the aspect ratio, $\xi = \frac{R_o}{a_o}$.

We will first consider neutral tori, in which Laplace pressure, Δp, will force toroidal droplets to shrink and/or break. In general,

$$\Delta p(\vec{r}) = 2\gamma H(\vec{r}) = 2\gamma(\kappa_1(\vec{r}) + \kappa_2(\vec{r})) \tag{1}$$

where γ is the surface tension between the liquid making up the toroidal drop and the continuous phase it is suspended in, H is the mean curvature, and κ_1 and κ_2 are the principal curvatures. The vector $\vec{r}$ identifies a point on the surface of a torus.

Since $H \neq 0 \ \forall \vec{r}$, we expect toroidal droplets to evolve in remarkable ways to eventually try to become spherical. In the presence of a constant voltage however, the uneven charge distribution on the surface results in additional stresses that will further contribute to the evolution of the drop.

II. MAKING CHARGED TOROIDAL DROPS

We generate our toroidal droplets using a rotating stage, on top of which we place a transparent cubic cuvette filled with the outer fluid. Through a set of clamps, a stand holds a needle that is partially immersed inside the bath, at a distance R_o from the rotation axis. Its position can be easily tuned using a micromanipulator.
Connected to the needle through a tube, we use a syringe and a pump to inject the inner fluid at a certain flow rate. When the fluid is pumped through the needle, due to the viscosity and the speed of the outer fluid around the tip of the needle, a jet is formed, and due to the imposed rotation of the stage, it closes onto itself after a full rotation, creating a toroidal drop. [1] If more volume is pumped after the toroid is formed, the fluid will be directly injected inside the torus, increasing the value of a_o (see Fig.1b).
For charged tori experiments, we need a high voltage power supply that sets the potential through a wire attached to the metallic needle.
Lastly, in order to monitor the evolution of the droplets, we use two CCD cameras; the first one pointing towards the zenith below the cuvette, and the other oriented to capture the evolution along the z-axis (see Fig.1a).

III. NEUTRAL TORI

We start by noting that toroidal and cylindrical jets share common features; they both have a circular cross section, and break into droplets provided their length to tube ratio is large enough. We thus begin by introducing breakup in cylindrical jets.

A. Theoretical treatment of cylindrical jets

The theoretical study of Rayleigh-Plateau consists in a linear stability analysis of the straight jet state, based on applying a sinusoidal perturbation to a perfectly symmetric and infinite cylindrical jet that is comprised of an inviscid and incompressible fluid [2].

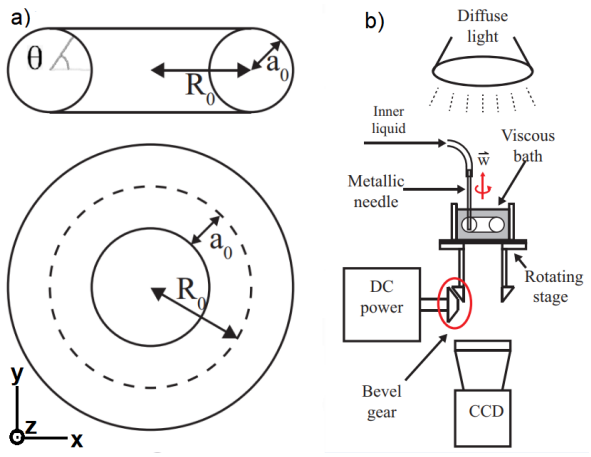

FIG. 1: a) Schematic of the torus measurements and parameters, with a_o the tube radius, R_o the centre torus radius, θ the inner angle, and the xyz coordinate system. b) Schematic of the setup used to generate toroidal drops with a needle inside a viscous bath rotating at angular velocity ω. We have used a diffuse light to obtain a better image contrast.

In this case, for small times, the radius will be $A(z,t) = a + \varepsilon\, e^{\omega t + ikz}$, where a is the initial radius, ω is the growth rate of the instability, and $k = \frac{2\pi}{\lambda}$ is the wavenumber associated to the perturbation, with λ the wavelength (see Fig.2).

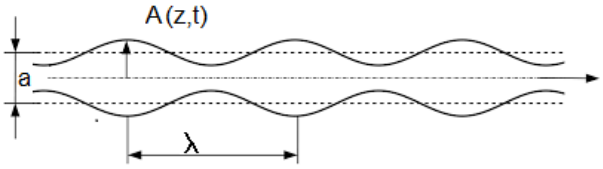

FIG. 2: Sketch of the jet perturbation $A(z,t)$, with λ the wavelength, and a the initial radius

Since $\varepsilon \ll a$, for small times we can ignore second and higher order terms in ε. Introducing our perturbation into the Navier-Stokes equation, results in the dispersion relation:

$$\omega^2 = \frac{\gamma}{\rho a}(ka)(1-(ka)^2)\frac{I_1(ka)}{I_0(ka)} \tag{2}$$

where I_0 and I_1 are the zero and first order Bessel functions of the first kind.
Our dispersion relation tells us which mode, corresponding to a particular value of ka, is most likely to cause breakup. The fastest unstable mode then corresponds to the maximum in the dispersion relation.
Note that there are no unstable modes for $ka > 1$, since in this case $\omega^2 < 0$, which is not possible for real ω; this corresponds to a stable situation for which no unstable modes can develop. Thereby, the Rayleigh-Plateau criterion provides a threshold wavelength below which no instability develops: $\lambda < 2\pi a$.

In 1935, S.Tomotika [3] performed a similar stability analysis but for the case of a jet with viscosity μ_i immersed in a bath of viscosity μ_o. Through the same reasoning, he obtained:

$$\omega = \frac{\gamma}{2a\mu_o}\left(1-(ka)^2\right)\Phi\left(ka, \frac{\mu_i}{\mu_o}\right) \tag{3}$$

where Φ is a function that depends on the mode dimensionless wavenumber ka and the viscosity ratio $\frac{\mu_i}{\mu_o}$. The values corresponding to the fastest unstable mode are tabulated, and through interpolation, one obtains the result shown in Fig.3.

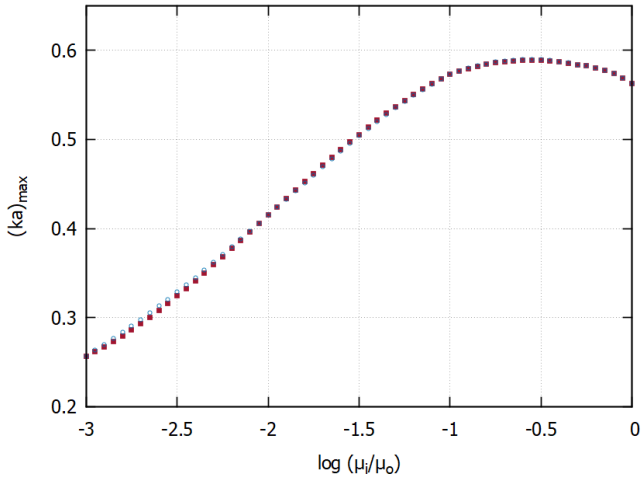

FIG. 3: Interpolation of the fastest unstable mode with the tabulated values obtained by Tomotika in his paper [3].

We can see that this dispersion relation scales differently than that in Eq.2. It depends on the dynamic viscosity of the outer fluid, which delays breakup. In the inviscid case, $\omega \sim \sqrt{\frac{\gamma}{\rho a}}$.

B. Toroidal analogy and experimental results

We apply the reasoning for cylindrical jets to a torus by considering it as a closed cylindrical jet. The resultant periodicity requires that the wavelength is related to the overall radius of the torus through $2\pi R_o = n\lambda$, where n is the number of droplets; that is to say that the torus must fit an integer number of wavelengths for it to break. From the previous relation, it follows that:

$$n = \frac{2\pi}{\lambda}R_o = kR_o = (ka_o)\,\xi \approx (ka_o)_{max}\,\xi \tag{4}$$

This assumes the mode that causes breakup is $(ka_o)_{max}$, as it is the fastest amidst all possible modes.

Using our experimental setup with a 60.000 cSt silicon oil as outer fluid, and 53 w/w glycerol in water

as inner fluid, corresponding to $\mu_i/\mu_o \approx 1/60$, we expect $(ka_o)_{max} \approx 0.48 \pm 0.2$.
Plotting the number of drops observed experimentally after breakup in terms of the aspect ratio, we obtain Fig.4.

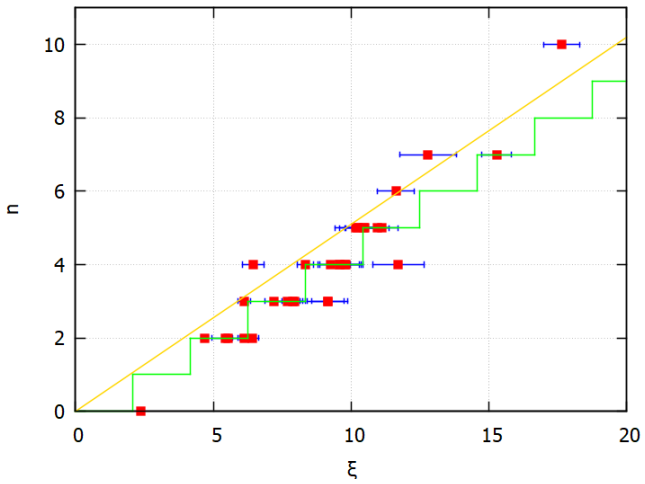

FIG. 4: Experimental data with the measurement uncertainty, linear regression line ($y = 0.51\,x$) and step function theoretical prediction ($y = 0.48\,x$)

Considering the leftmost points for each n, a linear fit of the data results in a slope corresponding to $(ka)_{max} = 0.51 \pm 0.04$, in great agreement with our theoretical expectations.

But, what if $(ka_o)_{max}\,\xi$ is not an integer?
From a mechanical point of view, the pressure drop inside the droplet between $\theta = 0$ and $\theta = \pi$ (see Fig.1a), is:

$$p_{in}(\pi) - p_{in}(0) = \frac{\gamma}{a_o}\frac{2\xi}{\xi^2 - 1} > 0 \qquad (\forall\, \xi > 1) \tag{5}$$

This implies that a torus will tend to reduce its inner radius, leading to a reduction of the aspect ratio. This amounts to shrinking which will be more evident in thick tori, as $(p_{in}(\pi) - p_{in}(0)) \to \infty$ as $\xi \to 1$.

This shrinkage explains the steps in Fig.4 and that we find the same n for a range of ξ-values; the torus generally shrinks until it can fit a given number of droplets for it to break through the fastest unstable mode.

IV. CHARGED TORI

In this section, we will discuss the effects of electrical stresses due to charging a toroidal droplet at constant voltage. To a first approximation, we will think of this as charging a perfect conductor. We will see that electrical stresses compete with surface tension stresses. Therefore, as a means to enhance the effects of charging, we will use two surfactants to significantly lower γ. The outer fluid is a 2% by mass of 65 cSt of aminopropyl terminated silicone (ATSO) in 60.000 cSt silicon oil, and the inner fluid is a mixture of 16 mM sodium dodecyl sulfate (SDS) in water, which also serves to increase the electrical conductivity of this liquid.

A. From shrinking to expanding

If we consider adding charge on a toroidal droplet, similar to H changing across the surface of the torus, charge will not be uniformly distributed due to the non-uniform electrostatic interactions between different parts of the toroidal surface. If we consider the cross section of the torus, the electrostatic repulsion that will feel charges near the centre will be more appreciable than those in the most external perimeter. Thereby, these uneven electrical and surface tension stresses will compete, resulting in novel dynamic evolution and richer phenomena.

All our experiments have been performed at constant voltage, which we impose by keeping the needle in contact with the droplet as it evolves. As long as the droplet is equipotential, charge must be located at the surface, leading to an electrical stress produced by the electric field due to the surface. The electrical stress, $\vec{\tau}_E = \frac{1}{2}\sigma_q \vec{E}_o$, points perpendicularly outwards to the interface, as $\vec{E}$ is also perpendicular to it. In this expression, σ_q is the surface charge density at each point, which can be written as $\sigma_q = \epsilon_r \epsilon_o \vec{E}_o \cdot \hat{n}$, with $\hat{n}$ the normal vector to the surface, ϵ_o the vacuum permittivity, and ϵ_r the relative permittivity of the inner fluid. Hence:

$$\vec{\tau}_E = \frac{1}{2}\epsilon_r \epsilon_o |E_o|^2 \hat{n} \tag{6}$$

which is along $\hat{n}$, regardless of the sign of the charge located at the surface. Together with surface tension stresses, the Laplace pressure is:

$$p_{in} - p_{out} = 2\gamma H - \frac{1}{2}\epsilon_r \epsilon_o |E|^2 \tag{7}$$

This equation tells us that surface tension effects can be reverted provided that we have enough surface charge density. Furthermore, we can see in Fig.5 that after a certain time from the application of the voltage on the droplet, these begin to expand, and this expansion hinges on the applied voltage and the aspect ratio.
Although we know the analytical expression of the mean curvature at every point, the electric field is far more complicated to compute as we have to consider the peculiar topology of the torus to solve Laplace's equation in toroidal coordinates with proper boundary conditions [4]. However, we can consider the pressure difference

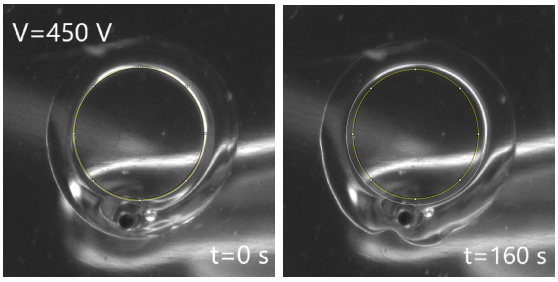

FIG. 5: Torus before applying the voltage, to which we have drawn a circumference delimiting the inner radius. Second image is the same torus 160 seconds later, where we can see that the inner radius has expanded.

$p_{in}(\pi) - p_{in}(0)$, as we did before. The transition between shrinking to expanding can be considered to be between surface tension and electrical stresses at these two locations.
Rearranging terms of Eq.7, one can obtain [4]:

$$\tilde{p}_{int} - \tilde{p}_{out} = \frac{\xi - 2\cos\theta}{\xi - \cos\theta} - N_E \tilde{E}^2(\xi, \theta) \tag{8}$$

where $\tilde{p}_{int}$ and $\tilde{p}_{out}$ are the dimensionless pressures inside and outside the surface, $\tilde{E}$ the dimensionless electric field, and $N_E = \frac{\epsilon_o \epsilon_r V^2}{2\gamma a_o}$ the electrocapillary number, which expresses the relative strength of electrical stress with respect to surface tension stress. The transition occurs when the pressure drop inside the droplet is null, hence:

$$N_E^{crit}(\xi) = \frac{\frac{2\xi}{\xi^2 - 1}}{\tilde{E}^2(\xi, \pi) - \tilde{E}^2(\xi, 0)} \tag{9}$$

This is the critical electrocapillary number, and is related to the transition through:

$$V(\xi) = \sqrt{\frac{2\gamma a_o N_E^{crit}(\xi)}{\epsilon_o \epsilon_r}} \tag{10}$$

The experimental results have been plotted in Fig.6. Note that shrinking dominates for small ξ; we need larger and larger V to revert shrinking into expanding, as far as surface tension effects become dominant as $\xi \to 1$. Similarly, decreasing ξ at constant V eventually reverts expanding, driven by the electric field, into shrinking.

B. Viscous fingering and dendritic behaviour

Further increasing the voltage, we can see that the interface distorts slightly, eventually leading to the formation of finger-like patterns along its perimeter.
These fingers can be understood as a Saffman-Taylor instability. Saffman and Taylor published in 1958 a paper [5] aiming to explain the formation of patterns

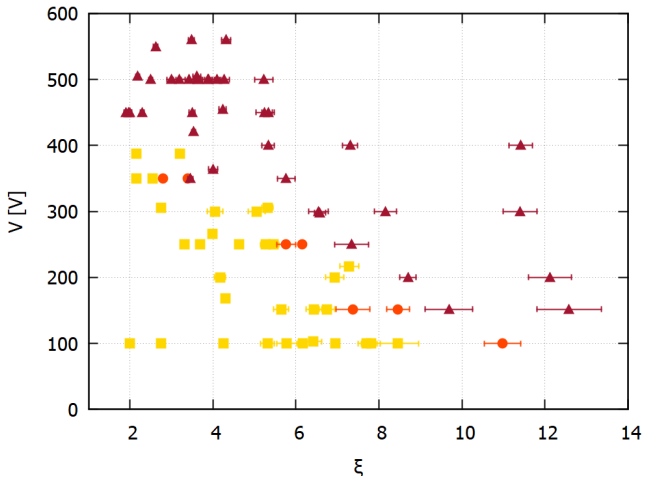

FIG. 6: Data obtained for different aspect ratio and different voltages, where ■ correspond to shrinking tori, ▲ to expanding, and ● do not show neither shrinking nor expanding behaviour.

when a fluid displaces another one with a higher viscosity in the interface of a confined quasi-two-dimensional space, known as a Hele-Shaw cell. Originally, Hele-Shaw cells were introduced as a simple method to perform experiments at low Reynolds numbers, and they consists of two parallel plates separated a distance b filled with the highly viscous fluid that is displaced by the inner fluid, which is pumped either at one of the edges of a longitudinal cell, or at the center of the upper plate of a radial cell. It was seen that as soon as the inner fluid was pumped, the viscous bath drags behind it, leading to the formation of the so-called viscous fingering. [6]

To connect these experiments with our charged tori, the idea is that the mechanical stress performed when pumping in Hele-Shaw cells is replaced by the electrical stress due to the charge distributed on the surface of our drops.

We have experimentally found that the more voltage we apply, the more fingers we observe, and the faster they expand (see Fig.7).
Since the expansion rate is controlled by the pressure drop at the interface, and thus V, due to Eq.7, it is reasonable that the timescale for finger growth increases with the voltage applied.
The number of fingers, n_{max}, can be estimated using a mapping to the theory for radial Hele-Shaw cells [7]. By linearly perturbing the uniform interface state, one can obtain the mode most likely to be seen.

$$n_{max} = \sqrt{\frac{1}{3}\left(\frac{12\mu_o}{\gamma}\left[U_o\left(\frac{\xi+1}{2}\right)^2\right] + 1\right)} \tag{11}$$

where U_o is the expansion velocity of the interface.
This equation shows that the number of fingers increases as the velocity increases, and due to Eq.7, the number

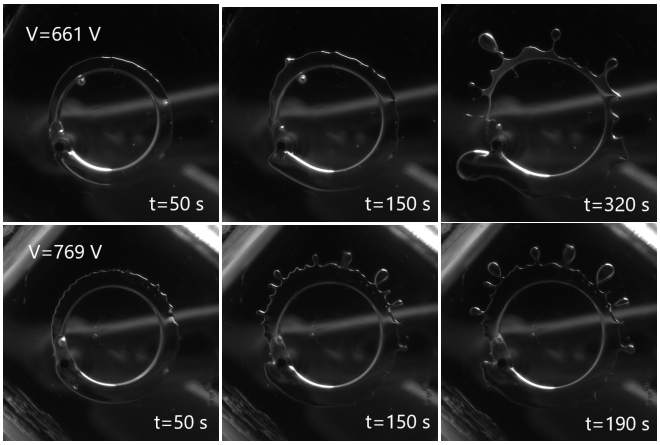

FIG. 7: Time evolution of the perturbation in two tori with the same aspect ratio and different voltage. The frames on top correspond to a 661 V torus while the second correspond to 769 V.

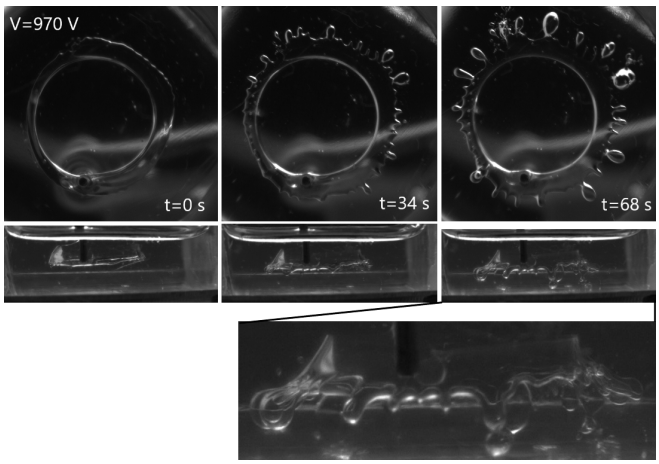

FIG. 8: Time evolution in the yz and xy planes of a toroidal droplet to which we applied 970 V. High voltages resulted in dendritic growth depicted in the upmost part of the top right image (t = 68 s). Note that the finger-like pattern expands along the 3^{rd} dimension of space, as shown in the zoomed image at the bottom.

of fingers will increase as the voltage increases.

As a final remark, it can be seen that, similarly to what happens in radial Hele-Shaw cells when large pressure is applied, large voltages result in the growth of dendritic interfaces similar to fractal patterns (see Fig.8). Interestingly, for the case of radial Hele-Shaw cells it has not been proved yet that the perimeter of the interface is fractal [6].

V. CONCLUSIONS AND FUTURE STEPS

We have seen that neutral tori obey the linear stability analysis developed by Tomotika, and that they shrink towards the centre as predicted theoretically after considering the pressure drop inside the torus.

The data from shrinking-expanding transition in Fig.6 presents a similar behaviour to experiments performed in [4].
We note, however, that once we reach a certain voltage ($\approx$ 450 V), drops tend to expand regardless of their aspect ratio. This is likely due to the low γ of our system, which would require values of ξ very close to 1, at these voltages, for shrinking to be dominant.

We have been able to see a novel 3-dimensional growth of viscous fingers. Perhaps, these behaviour might be explained because of the density difference between the inner and outer fluid, and thus, might be related to sinking.

Further research should be done in the dendritic regime. Due to the minute sizes and the accuracy required to calculate a possible fractal dimension, an improvement on imaging is a must.

Acknowledgments

I would like to express my gratitude to Alberto Fernández-Nieves and Jyothishraj Nambisan for their support, advisory and guidance throughout this project. Last but not least, I would like to thank my family, partner and friends for their patience and motivation, without whom nothing would have been possible.

[1] E. Pairam and A. Fernandez-Nieves, *Generation and stability of toroidal droplets in a viscous liquid*, Phy. Rev. Lett., **102**, 234501 (2009).
[2] A.A. Fragkopoulos et al, *Teaching Rayleigh-Plateau instabilities in the laboratory*, Eur. J. Phys., **36**, 055023 (2015).
[3] S. Tomotika, *On the instability of a cylindrical thread of a viscous liquid surrounded by another viscous fluid*, Proc. R. Soc. Lond., **150**, 322, pp.322-337, (1935).
[4] A.A. Fragkopoulos, *Toroidal Instabilities in the Presence of Charge and Non-Newtonian Fluids*, Eur. J. Phys., **36**, 055023, (2017).
[5] P.G. Saffman and G.I. Taylor, Proc. R. Soc. A, **245**, 312, (1958).
[6] T.Vicsek, *Fractal Growth Phenomena*, WSPC, 2nd ed., pp.294-300, (1992).
[7] A.A.Fragkopoulos, A.Fernandez-Nieves and A.Aizenman, *Charge-Induced Saffman-Taylor Instabilities in Toroidal Droplets*, Phy. Rev. Lett., **118**, 264501, (2017).